Secondary formation and impacts of gaseous nitro-phenolic compounds in the continental outflow observed at a background site in South China

Yi Chen [1,2], Penggang Zheng [1,2], Zhe Wang [1,], Wei Pu [2], Yan Tan [2], Chuan Yu [2], Men Xia [2], Weihao Wang [2], Jia Guo [3], Dandan Huang [4], Chao Yan [5], Wei Nie [6], Zhenhao Ling [7], Qi Chen [8], Shuncheng Lee [2], Tao Wang [2]*

[1] Division of Environment and Sustainability, The Hong Kong University of Science and Technology, Hong Kong SAR, 999077, China

[2] Department of Civil and Environmental Engineering, The Hong Kong Polytechnic University, Hong Kong SAR, 999077, China

[3] Research Center for Eco-Environmental Sciences, Chinese Academy of Sciences, Beijing 100085, China

[4] State Environmental Protection Key Laboratory of Formation and Prevention of Urban Air Pollution Complex, Shanghai Academy of Environmental Sciences, Shanghai, 200233, China

[5] Institute for Atmospheric and Earth System Research / Physics, Faculty of Science, University of Helsinki, Helsinki, 00014, Finland

[6] Joint International Research Laboratory of Atmospheric and Earth System Research, School of Atmospheric Sciences, Nanjing University, Nanjing, 210023, China.

[7] School of Atmospheric Sciences, Sun Yat-sen University, Zhuhai, 519000, China

[8] State Key Joint Laboratory of Environmental Simulation and Pollution Control, BIC-ESAT and IJRC, College of Environmental Sciences and Engineering, Peking University, Beijing, 100871, China

Abstract

Nitro-phenolic compounds (NPs) have attracted increasing attention because of their health risks and impacts on visibility, climate and atmospheric chemistry. Despite many measurements of particulate NPs, the knowledge of their gaseous abundances, sources, atmospheric fates, and impacts remains incomplete. Here, eighteen gaseous NPs were continuously measured with a time-of-flight chemical ionization mass spectrometer at a background site in South China in autumn and winter. Abundant NPs were observed in the continental outflows from East Asia, with a total concentration up to 122.1 pptv. Secondary formation from the transported aromatics dominated the observed NPs, with mono-NPs exhibiting photochemical daytime peaks and nighttime enrichments of di-NPs and Cl-substituted NPs. The budget analysis indicates that besides the •OH oxidations of aromatics, the NO_3• oxidation also contributed significantly to the daytime mono-NPs, while the further oxidation of mono-NPs by NO_3• dominated the nocturnal formation of di-NPs. Photolysis was the main daytime sink of NPs and produced substantial HONO, which would influence atmospheric oxidation capacity in downwind and background regions. This study provides quantitative insights on the formation and impacts of gaseous NPs in the continental outflow and highlights the role of NO_3• chemistry in the secondary nitro-aromatics production that may facilitate regional pollution.

Synopsis

Atmospheric oxidation boosts the production of nitro-phenolic compounds from the continental origin, potentially impacting the air quality over southern China.

Keywords: *nitro-phenolic compounds, photochemical oxidation, nocturnal chemistry, continental outflow, HONO production*

Graphic for Table of Contents (TOC)

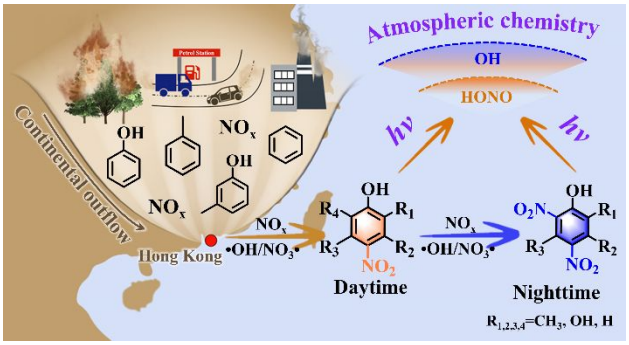

1 Introduction

Nitro-phenolic compounds (NPs) are aromatic compounds with both nitro (-NO_2) and hydroxyl groups (-OH) connecting to a benzene ring. They are important atmospheric pollutants that have been proved to be phytotoxic and genotoxic [1], and are key components of brown carbon that affect the visibility and climate [2-5]. Furthermore, the photolysis of NPs can produce HONO and OH radicals to increase the atmospheric oxidation capacity [6-9]. Owing to the significance of NPs on air quality and ecosystems, plenty of studies have focused on their distribution, sources, sinks and impacts in the atmosphere [1, 5, 10-12].

Both primary emission and secondary formation of NPs have been reported in laboratory and field experiments. Coal combustion, biomass burning (BB), and vehicle exhaust are predominant primary sources of particulate NPs, the emission rates of which are affected by both the fuel types and combustion conditions [13-15]. Significant contributions of 4-nitrophenol and methyl-nitrophenols from coal combustion, and 2,6-dimethyl-4-nitrophenol and 4-nitrocatechol from BB have been observed in fine particles at urban Jinan in north China [11]. Vehicle emission and domestic heating were reported as important contributors to the particulate NPs measured in Strasbourg, France [12]. Moreover, many studies promulgated the importance of secondary formation of NPs in the atmosphere, especially in the photochemical season [16]. Field measurements at a rural village of Germany[17] and urban Hong Kong [18] both reported that abundant NPs in the particle phase were dominated by the photooxidation of BB precursors. Elevated particulate NPs

from secondary formation under high NO_x and anthropogenic VOCs conditions were also observed in urban Beijing [10].

Generally, the secondary NPs was produced from the oxidation of aromatics by •OH or NO_3• in the presence of NO_x, which has been evidenced in the laboratory and quantitative theory calculation [19-25]. Aromatic hydrocarbons oxidized by •OH and NO_3• would generate -OH substituted aromatics such as cresol [26]. The further oxidation of -OH substituted aromatics generates phenolic radicals, which combine with NO_2 to form NPs [19-21, 25]. The reaction rate coefficients of -OH substituted aromatics with NO_3• or •OH are high up to 10^{-11}~10^{-10} cm^3 $molecule^{-1}$ s^{-1}, which leads to a fast generation of NPs once -OH substituted aromatics presenting in the atmosphere [23, 24, 27]. In addition to the gas-phase oxidation, aqueous-phase oxidation of aromatics were also suggested as important formation pathways for some NPs [28], such as 4-methyl-5-nitrocatechol at urban Beijing [10]. After generated in the atmosphere, NPs could be consumed fast by further oxidation and photolysis, resulting in a short lifetime for NPs in the daytime [6, 7, 9, 29-31].

Most of the previous field studies focused on particulate NPs [10, 13, 15, 18, 32], and several studies have pointed out that some NPs may present similar or even higher concentrations in the gas phase [11, 29, 33, 34]. More quantitative determination of gaseous NPs is essential to obtain a better understanding on the fates and the impacts of NPs in the atmosphere. Moreover, because of the fast generation and photochemical consumption of different NPs [19], continuous and online measurement is necessary and desirable. Recent studies utilizing high-resolution time-of-flight

chemical ionization mass spectrometers (Tof-CIMS) and proton-transfer-reaction time-of-flight mass spectrometer (PTR-Tof-MS) have observed abundant gaseous NPs at Uintah Basin [29], urban Beijing [34, 35], Dezhou [36], and Taizhou [37], and indicated the importance of secondary formation of some NPs species from urban and BB emissions. However, a comprehensive understanding of the formation and transformation of NPs away from urban source regions, and their impacts in regional or larger scales remain elusive.

In this study, we conducted a field campaign at a regional background site in Hong Kong to quantitatively characterize the gaseous NPs in the outflow air from the urbanized regions. The diurnal variations, sources and sinks of eighteen gaseous NPs were comprehensively investigated. The atmospheric budgets, formation mechanisms at the molecular level, and implications of NPs on regional atmospheric chemistry were further evaluated with a photochemical box model.

2 Experimental Methods

The field campaign was conducted in a regional background monitoring station (Cape D'aguilar, 22.22˚N, 114.25˚E, 60 m above sea level, Figure S1) in Hong Kong from 20 September to 8 October and 1 November to 18 December in 2018. The site is located in the southeastern tip of Hong Kong Island, and isolated by hills from the urban center. The air quality in the station is generally influenced by the continental outflows from the North and East China due to the Asian monsoon, transported emissions from urban Hong Kong and Pearl River Delta (PRD) region, oceanic air mass from the South China sea, and biogenic emissions from local vegetation [38, 39].

During the field campaign, a nitrate-based Tof-CIMS (NO_3^--Tof-CIMS, Aerodyne) was used to measure the gaseous NPs. Volatile organic compounds (VOCs) were measured by a PTR-QMS or a PTR-Tof-MS for the two-phase campaigns. N_2O_5 was measured by a quadrupole CIMS (Q-CIMS, THS Instruments). The trace gases (NO, NO_2 O_3, SO_2 and CO), $PM_{2.5}$ mass concentration, and meteorological parameters were also measured. Detailed information on the instruments can be found in our previous works [40, 41].

Within the Tof-CIMS, multifunctional organics (M) in the atmosphere react with the primary ion (i.e., NO_3^-), and then can be measured in the form of $M(HNO_3)_nNO_3^-$ (n=0,1) cluster ions and deprotonated ions of M^- by mass spectrometer. The obtained data were analyzed with Tofwerk software (version 3.2.0). Mass calibration was performed with 61.9884 (NO_3^-), 124.9840 ($HNO_3NO_3^-$), 187.9797 ($(HNO_3)_2NO_3^-$), 201.0153 ($C_6H_5NO_3(NO_3)^-$) to ensure accuracy of mass detection within 5 ppm. The average mass resolution of Tof-CIMS was 5200 for m/q>200 during the whole campaign, and the high-resolution peak-fitting allowed more precise molecular identification of measured organic compounds. A recent study employing the same type of instrument and configuration has identified and quantified six classes of NPs in Beijing [34]. Similarly, we identify eighteen NPs species as summarized in Table S1, and Figure S2 illustrates the high-resolution peak fittings of some typical NPs. Detailed descriptions of the instrument and data analysis are provided in supporting information (SI).

Sensitivity calibration was performed with 2-nitrophenol and 4-nitrophenol by using the standard gas generated from certified permeation tubes. The sensitivity of 2-nitrophenol was too low to be

measured by the Tof-CIMS in the present study, and the sensitivity of 4-nitrophenol was determined to be $9.13\pm0.21\times10^{-4}$ ncps/ppt (Figure S3). Thus, the measured signal of $C_6H_5NO_3$ in Tof-CIMS should be dominated by 4-nitrophenol. Because of the uncertainty of the structure and unavailable of commercial standards for other NPs, the instrumental sensitivity of 4-nitrophenol was also applied to other NPs, with the correction of mass-dependent transmission efficiency. 2-methyl-4-nitrophenol has been calibrated previously by Yuan et al. [36] and Cheng et al. [34], and their results showed a slightly higher or lower sensitivity of 2-methyl-4-nitrophenol than that of 4-nitrophenol, respectively. The uncertainty introduced by using the uniform sensitivity with mass-dependent transmission correction was estimated to be 40%.

An observation-based photochemical box model (PBM) built on the Master Chemical Mechanism (MCM v3.3.1) (http://mcm.york.ac.uk) was employed to investigate the budget and formation of different NPs [29, 34, 36], as well as their impacts on HONO formation. This PBM has been used in our previous studies [42, 43]. The gas-phase inorganic and organic reactions, kinetic data and parameters were extracted from MCM v3.3.1. The reaction pathways of production and loss of different NPs were included in the model and are explicitly summarized in scheme S1 and S2 in the SI. Besides, the photolysis of NPs, a gas-particle partitioning module of NPs following Johnson et al. [44], and different HONO formation reactions are also considered and embedded in the model to comprehensively explore the fates of NPs and their impacts in the atmosphere. The PBM was constrained with the measurement data of trace gases, key VOC species, and meteorological parameters. More details about the model configuration are provided in the SI.

3 Results and Discussions

3.1 Overview of nitro-phenolic compounds

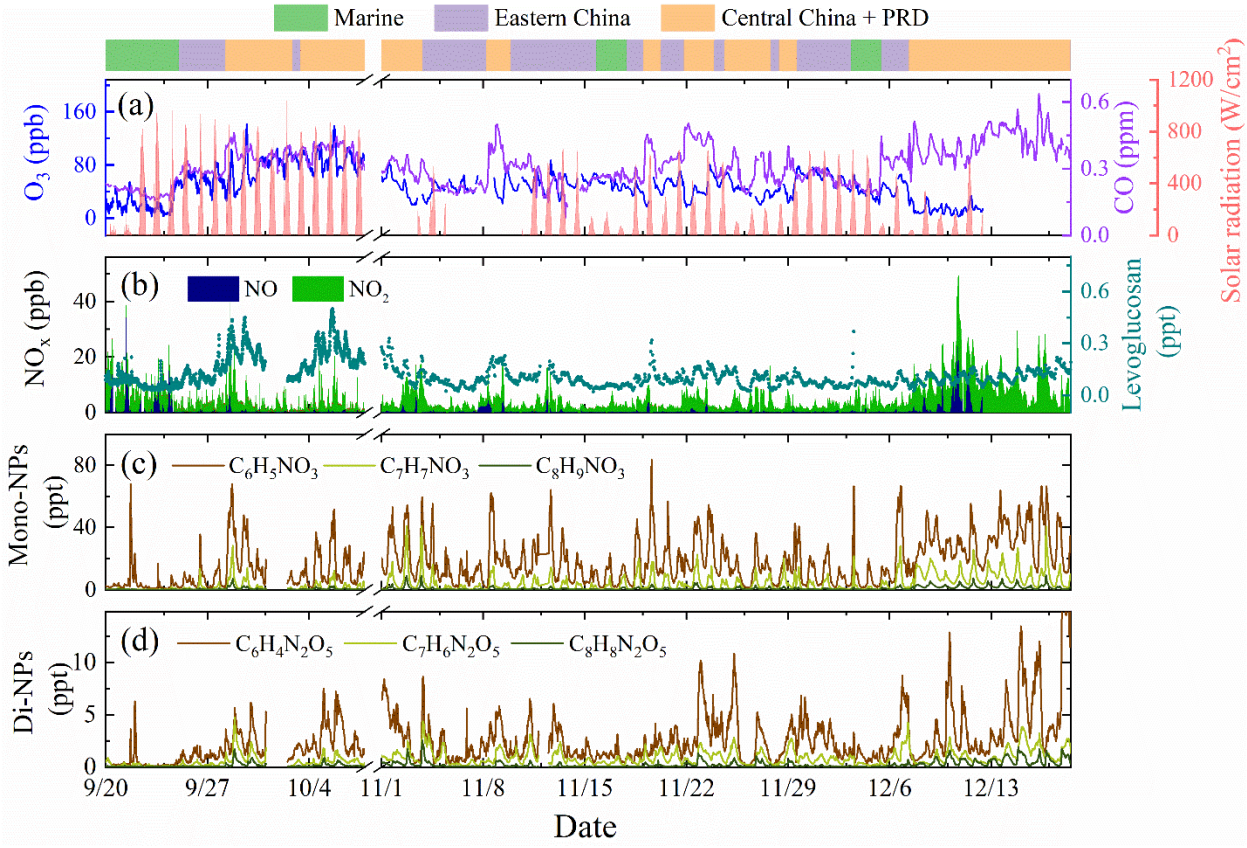

Figure 1. Time series of O_3, CO and solar radiation (a), NO_x and levoglucosan (b), $C_6H_5NO_3$, $C_7H_7NO_3$, $C_8H_9NO_3$ (c), $C_6H_4N_2O_5$, $C_7H_6N_2O_5$, $C_8H_8N_2O_5$(d) measured in this field campaign. In the top of this figure, periods marked in green, purple and orange represent three clusters classified from backward trajectory analysis.

During the campaign, eighteen kinds of NPs were measured continuously, including twelve kinds of mono-nitro-phenolic compounds (mono-NPs) with 1 to 3 -OH substituted groups, four di-nitro-phenolic compounds (di-NPs) with 1 to 2 -OH substituted groups, and two mono-NPs with -Cl substituted group (Cl-NPs). The time series of the key NPs, together with trace gases, and

meteorological parameters, are shown in Figure 1, S4 and S5, and the statistical summary of their concentrations is shown in Figure 2a and summarized in Table S1. Among the measured NPs, $C_6H_5NO_3$ was the most abundant species, with an average (± one standard deviation) and maximum concentration of 16.9±14.6 pptv and 84.0 pptv, respectively. It was followed by $C_7H_7NO_3$ and $C_6H_4N_2O_5$ with the average concentrations of 4.0±5.2 pptv and 2.5±2.5 pptv, respectively. $C_6H_4NO_3Cl$ and $C_6H_3NO_3Cl_2$ were measured in the gas phase for the first time and confirmed by checking their isotopic ratios (see SI), showing concentrations up to 1.2 and 0.88 pptv during the nighttime, respectively. Generally, the concentration of gaseous NPs decreased with the increase of -NO_2, -OH substituted groups and carbon numbers. The NPs in the same category showed a similar temporal pattern and good correlations (Figure S6), indicating their similar sources and atmospheric processing. The mean concentrations of NPs measured at Cape D'aguilar in this study were much lower than those measured at urban regions, where significant anthropogenic emissions (e.g., Beijing, Santiago, Milano) or biomass/crop residue burning (e.g., Dezhou, Taizhou) dominated the NPs concentrations [32, 34, 36, 37, 45]. However, the NPs measured at this regional background site were higher than that detected in the rural site of Lombardia and in the Horse Pool site at Uintah Basin [29, 45], suggesting the potential contribution of photochemical secondary formation and significant influences of continental outflows.

Three-day (72 h) backward trajectories were reconstructed using the Hybrid Single-Particle Lagrangian Integrated Trajectory (HYSPLIT) model to investigate the origins of air masses arriving at the site and the influences on the variation of observed NPs. Throughout the

measurement period, continental outflows from East China along the coastline (cluster 2) and from Central China and the PRD region (cluster 3) dominated the air masses arriving at the site, with occasional marine airflow from the South China Sea (cluster 1) (Figure1 and S7). As shown in Figure 2b and Table S1, elevated concentrations of most NPs were found in cluster 3 from Central China and the PRD region, especially for $C_6H_5NO_3$, $C_7H_7NO_3$, $C_8H_9NO_3$, and $C_6H_4N_2O_5$, which showed 1.6 to 3.6 times and 4.1 to 8.2 times enhancement compared to the East China airflow and the marine airflow, respectively. The higher NPs concentrations are likely associated with the extensive anthropogenic emissions from Central China and the PRD region, which contributed to both higher primary emissions and secondary formation from the emitted precursors.

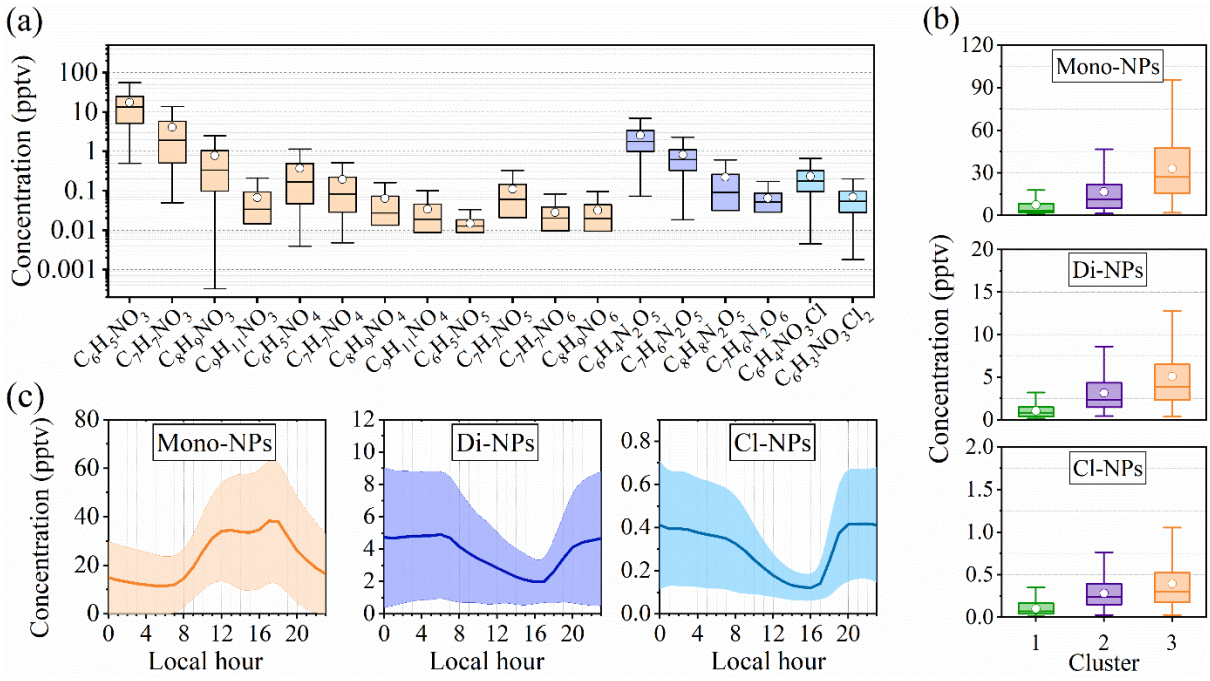

Figure 2. The average concentrations of measured NPs during the field campaign (a), the concentration distribution of mono-NPs, di-NPs and Cl-NPs in different trajectory clusters (b), and diurnal pattern of total mono-NPs, di-NPs, and Cl-NPs (c). In (a) and (b), the circle presents the

mean value, the line in the up, middle and bottle of the box plot represent 25%, 50% and 75% percentile point, respectively, the whiskers extend from each box to ±1.5×IQR (inter quartile range). The line and the shadow area in (c) represent the mean value and standard deviation, respectively.

3.2 Diurnal pattern and sources analysis

The diurnal variations of the measured NPs are shown in Figure 2c, S5 and S8. The mono-NPs exhibited a typical photochemical diurnal pattern, with a broad high peak from noon till early evening. It was noted that two local peaks were observed at around 11:00~13:00 and 17:00~18:00 for most of mono-NPs. This diurnal pattern is different from previous winter observations at Uintah Basin [29] and Beijing [35], where the mono-NPs exhibited night peaks and efficient loss in the daytime. An observation conducted in urban Beijing in the autumn reported clear noon-afternoon peaks for nitrocatechol and methylnitrocatechol, while other mono-NPs only show peaks in the early evening [34]. A similar noon peak contributed by photochemical formation was also observed at a rural site at Dezhou in north China during the non-BB episode periods [36]. Because of the fast photolysis loss of most of the NPs, the high daytime peaks persisting for the whole afternoon in the present study suggested a significant source from photochemical production, as direct emission from local combustion sources was minimal in this region. Di-NPs showed strong diurnal variation with high concentrations presented at nighttime, similar to previous observations at urban or rural areas [29, 34, 35], illustrating significant nocturnal generation or/and fast loss in the daytime. Cl-NPs

showed similar temporal variation and diurnal pattern as di-NPs, indicating a similar formation or/and loss mechanism.

Vehicle exhausts, coal combustion, and BB have been identified as potential sources for NPs or their precursors. The correlations of NPs with NO or SO_2, as respective indicators of vehicle emission and coal combustion, were weak ($R^2 < 0.14$) (Figure S6), suggesting that those two primary sources had a minor contribution to the observed NPs but likely account for the precursors of NPs formation. The better correlation of NPs with levoglucosan, a typical tracer of BB, and CO, a widely existing by-product from the combustion process (Figure S6), suggests more contributions of BB to the observed NPs. The correlations of the different classes of NPs with levoglucosan and CO in cluster 1 to 3 were shown in Figure S9 and S10, respectively. Those scatters grouped by clusters were observed with distinct concentration ranges and demarcations for different clusters. The concentrations of CO, levoglucosan and NPs stepped up from the airflow from marine to center China and PRD (cluster 1 to cluster 3). These results proclaim that BB from continental outflow was an important source for NPs formation in this region, consistent with the previous study of particulate NPs in Hong Kong [18]. However, as levoglucosan and CO were relatively inert and long-lifetime compounds in the atmosphere, the good correlations between them and NPs could not explicitly indicate whether NPs were dominated by the direct emission or secondary oxidation of precursors emitted from BB sources.

A tracer method analogous to the EC-tracer method used for secondary organic carbon calculation was adopted in this study to evaluate the contributions of primary emission and secondary

oxidation to the observed NPs [36, 46, 47]. CO and levoglucosan were selected as the tracer for combustion and BB, respectively. The secondary formation of mono-NPs was evaluated via equation (1),

$$[NPs]_s = [NPs]_t - \left(\frac{[NPs]}{[Tracer]}\right)_p \times [Tracer] \quad (1)$$

where $[NPs]_s$ and $[NPs]_t$ are the concentration of NPs generated from secondary oxidation and the total measured NPs, respectively, $\left(\frac{[NPs]}{[Tracer]}\right)_p$ is the primary emission ratio of NPs relative to the tracer, [Tracer] is the concentration of tracer. $\left(\frac{[NPs]}{[Tracer]}\right)_p$ was estimated from the fitting of the lowest 15% $\frac{[NPs]}{[Tracer]}$ ratios, assuming that the primary source dominated the period with minimal secondary formation.

The results from both tracers are consistent and demonstrate the dominant secondary formation of mono-NPs in the daytime, di-NPs and Cl-NPs at nighttime, respectively (Figure S11). As shown in Figure S11a, up to 81%-94% of $C_7H_7NO_3$ and $C_8H_9NO_3$ were contributed by the secondary formation in the daytime. For $C_6H_5NO_3$, the contribution of secondary formation was lower but still can reach around 80%. The fraction of secondary formation for mono-NPs started to decrease after sunset, down to around 10-30% before sunrise. Furthermore, it was noted that the time series of the increment of mono-NPs in the daytime (Δmono-NP) showed a similar trend as the increment of O_3 (ΔO_3) (Figure S12). The good correlations between ΔO_3 and Δmono-NPs (Figure S13) also confirm the importance of the photochemical oxidation for mono-NPs. As reported in previous studies, the photochemical formation of mono-NPs was related to the oxidation of aromatics in the presence of NO_2 [10, 22, 25, 29, 34]. Here, the relationships between mono-NPs and possible precursors

in the daytime were investigated in Figure 3a-3c and S14. The concentration of mono-NPs increased monotonically with the increase of aromatics, NO_2, and solar radiation, implying the enhanced mono-NPs formation with the increase of precursors [18].

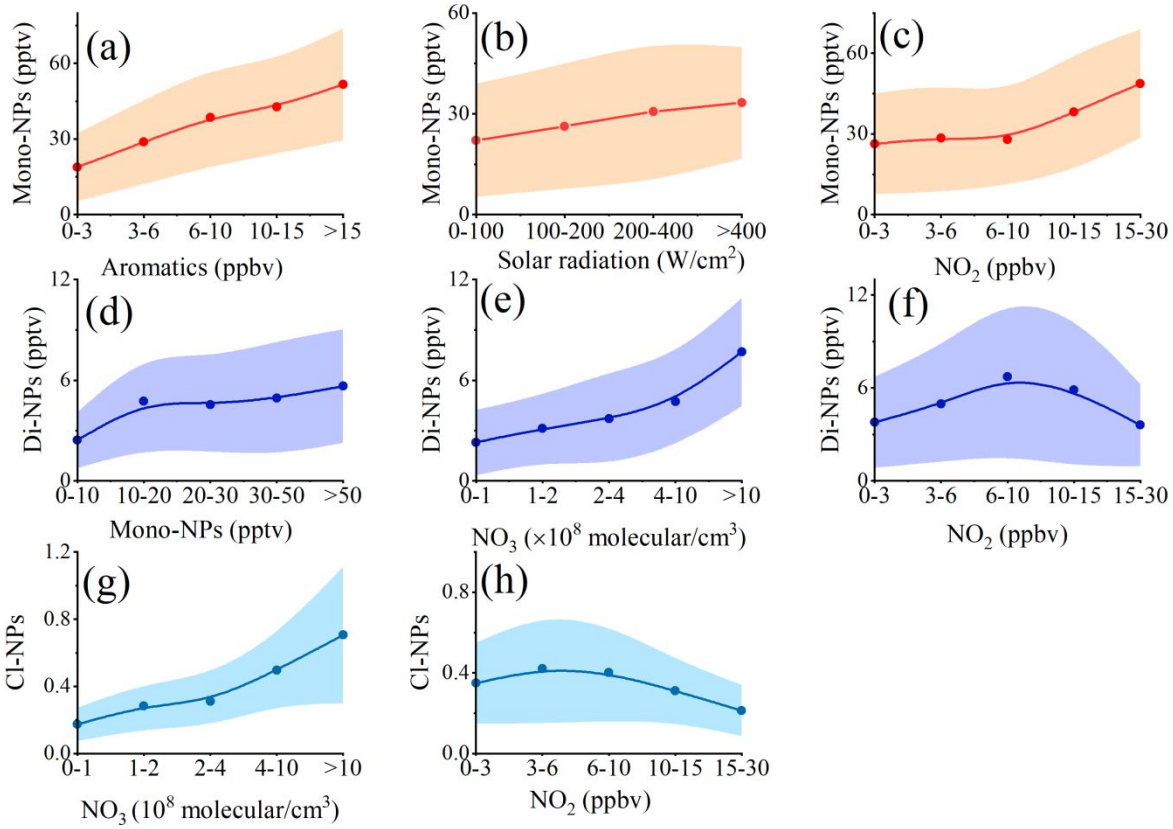

Figure 3. Concentration of Mono-NPs (the sum of $C_6H_5NO_3$, $C_7H_7NO_3$ and $C_8H_9NO_3$) as a function of aromatic hydrocarbon (the sum of benzene, toluene, xylene) (a), NO_2 (b) and solar radiation bins (c) in the daytime; concentration of Di-NPs (the sum of $C_6H_4N_2O_5$, $C_7H_6N_2O_5$, $C_8H_8N_2O_5$) as a function of Mono-NPs (d), NO_3• (e), NO_2 (f) concentration bins at night; concentration of Cl-NPs (the sum of $C_6H_4NO_3Cl$ and $C_6H_3NO_3Cl_2$) as a function of NO_3• (g), NO_2 (h) concentration bins at night.

In Figure S11b, secondary formation dominated the di-NPs concentrations at nighttime, and the secondary fraction decreased to around 20-30% for $C_6H_4N_2O_5$ and $C_7H_6N_2O_5$ in the afternoon. For $C_8H_8N_2O_5$, the secondary fraction was still higher than 50%, indicating the importance of secondary formation for di-NPs in the daytime though the concentration was low. As reported, the oxidation of mono-NPs by •OH and NO_3• in the presence of NO_2 was an important pathway for di-NPs formation [29, 48]. The transformation from mono-NPs to di-NPs was observed in our study. At around 18:00, the concentration of mono-NPs sharply decreased, while the generation of di-NPs started. The order of di-NPs concentrations was $C_6H_4N_2O_5 > C_7H_6N_2O_5 > C_8H_8N_2O_5$, which was consistent with the order of related mono-NPs. The nighttime concentration of di-NPs also clearly depended on the mono-NPs (Figure 3d, S15). However, the relationship of di-NPs with NO_2 showed a different pattern, with a maximum value around 6-10 ppbv of NO_2, and then decreasing with the increase of NO_2 (Figure 3f, S15). We further calculated the concentration of NO_3• with the measured N_2O_5 and NO_2 via the thermodynamic equilibrium equation between them [49, 50]. As shown in Figure 3e, S15 and S16a, the concentration of di-NPs was highly correlated with NO_3• concentration, indicating the significance of NO_3•-initiated oxidation in di-NPs formation. If considering the generations of $C_6H_4N_2O_5$, $C_7H_6N_2O_5$ and $C_8H_8N_2O_5$ were all contributed by $C_6H_3NO_3$, $C_7H_7NO_3$, $C_8H_9NO_3$, respectively, a transformation coefficient ($-\frac{\Delta_{di\text{ - }NP}}{\Delta_{mono\text{ - }NP}}$) could be obtained. As shown in Figure S17, the calculated transformation coefficients for $C_6H_4N_2O_5$, $C_7H_6N_2O_5$ and $C_8H_8N_2O_5$ were 0.068, 0.077 and 0.16, respectively.

The contribution of secondary formation to Cl-NPs was similar to the di-NPs, more than 70% in the nighttime and down to 20% in the afternoon (Figure S11c). Previous laboratory study on Cl-NPs formation was limited, and their detailed formation mechanisms remain unclear. Here we examine the relationship of Cl-NPs with NO_3• and NO_2 (Figure 3g, 3h, S16b). The trends of Cl-NPs with the increase of NO_3• and NO_2 were similar to that of di-NPs at nighttime, which also implied the importance of the NO_3• oxidation pathway on Cl-NPs formation. Chlorobenzene and dichlorobenzene that have been detected in many places may be the potential precursors for $C_6H_4NO_3Cl$ and $C_6H_3NO_3Cl_2$, respectively [51-53]. Once chlorobenzene and dichlorobenzene were emitted into the atmosphere, they could be oxidized by •OH or NO_3• to generate chlorophenol and dichlorophenol, respectively [54-56]. Chlorophenol and dichlorophenol also could be directly emitted from pesticide preparations and industrial exhaust [57, 58]. Then, chlorophenol and dichlorophenol could be further oxidized [31, 59], but no relevant studies have reported their oxidation products. A possible formation pathway for $C_6H_4NO_3Cl$ and $C_6H_3NO_3Cl_2$ could be the chlorophenol and dichlorophenol oxidation similar to the phenol oxidation with NO_2 presented to produce nitrophenol [19, 54]. In addition, Cl atom may react with aromatics to generate Cl-substituted aromatics [60, 61], serving as potential precursor of Cl-NPs. The reported low reaction rate and yield of Cl-substituted aromatics from benzene with Cl and phenyl radical with Cl_2 under ambient condition [61, 62] suggest only a minor contribution to the Cl-NPs formation. The research on the Cl atom oxidation of many key precursors (e.g., phenol) is still lacking, and thus the roles of Cl atom

on Cl-NPs formation are still poorly understood. Further studies are required to investigate the formation mechanisms of Cl-NPs in the real atmosphere.

3.3 Budget analysis with box model

Because the secondary formation was found to dominate the observed NPs in this campaign, PBM constrained with the measurement data was applied to further analyze their formations and budgets at the molecular level.

For mono-NPs, we focused on the formation of $C_6H_5NO_3$ and $C_7H_7NO_3$ owing to their higher concentrations among mono-NPs and more clear structures of them and their precursors. In model mechanism (MCM v3.3.1), $C_6H_5NO_3$ and $C_7H_7NO_3$ are generated from phenoxy (C_6H_5O•) and C_7H_7O• (including 2-methyl-phenoxy (TOL1O) and 3-methyl-phenoxy (MXYL1O) for 6-methyl-2-nitrophenol, and 4-methyl-phenoxy (PXYL1O) radical for 4-methyl-2-nitrophenol) reacting with NO_2, respectively. Besides the dry deposition and the oxidation by •OH and NO_3•, the consumption of $C_6H_5NO_3$ and $C_7H_7NO_3$ via photolysis was also added to the model. The photolysis of $C_6H_5NO_3$ and $C_7H_7NO_3$ has been controversial [6, 7, 9, 30, 31, 34, 63]. Bardini et al. and Bejan et al. reported that the photolysis rate of 2-nitrophenols and methyl-nitrophenols were 1.4% and 3.2%~7.1% of the photolysis frequency of NO_2 (J_{NO2}), respectively, while Sangwan et al. suggested that their photolysis rate could up to 2 folds of J_{NO2} [6, 7, 30, 63]. Hence, a sensitivity test with different photolysis rates (0-50% of J_{NO2}) was performed to test the simulation of NPs.

The comparison between observation and simulation was shown in Figure 4a, S18a, and S19a. The simulation results restored the strong diurnal variation of $C_6H_5NO_3$ and $C_7H_7NO_3$, affirming the

dominance of *in-situ* secondary production on their observed abundances. As expected, the simulated concentrations decreased with the increase of the photolysis frequency. The simulation result of 5% and 10% of J_{NO2} were more consistent with the observed results of $C_7H_7NO_3$, which is approximate to the obtained photolysis rates of methyl-nitrophenols by Bejan et al. [30]. However, the simulation of $C_6H_5NO_3$ was lower than the observation even when photolysis was excluded in the model. As discussed above, primary emission also contributed to $C_6H_5NO_3$ levels. However, though a more comparable result was found between the simulation and secondary fraction of $C_6H_5NO_3$ (from the tracer method), discrepancies still existed on some days (Figure S18a), which may be caused by several reasons. First, in view of the short lifetime of phenol, only secondary formation of phenol was considered in the model [64]. The possible primary emissions of phenol may partly explain the underproduction of $C_6H_5NO_3$ [34, 35, 64]. Second, the incomplete formation mechanism of $C_6H_5NO_3$ in the model may also account for the inconsistency, because only the formation mechanism of 2-nitrophenol was included in the MCM mechanism, while our measured $C_6H_5NO_3$ was likely dominated by 4-nitrophenol. Besides, O_3 was reported could affect the production ratio of 2-nitrophenol and 4-nitrophenol [19], and could even oxidize aromatics directly to produce -NO_2 substituted compounds in the presence of NO_2 [65], which was not considered in the model. The complicated but unclear formation mechanism of different NP species requires further comprehensive research.

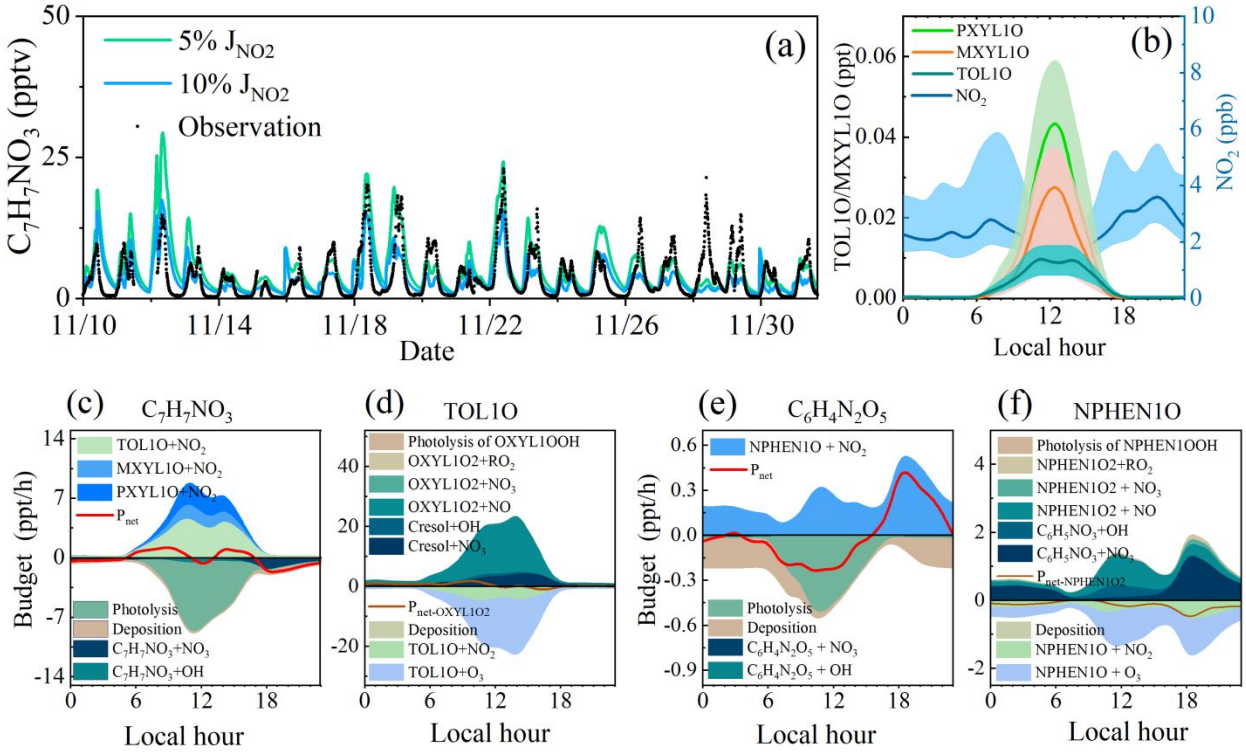

335

336 **Figure 4.** The comparison between the simulation and observation of $C_7H_7NO_3$ (a), diurnal

337 variation of TOL1O, MXYL1O, PXYL1O and NO_2 (b), budget of $C_7H_7NO_3$ (c) and TOL1O (d)

338 with 5% of J_{NO2} used for the photolysis rate, budget of $C_6H_4N_2O_5$ (e) and NPHEN1O (f) with 1.4%

339 of J_{NO2} used for the photolysis rate.

340 The main formation and consumption pathways of $C_6H_5NO_3$ and $C_7H_7NO_3$ derived from the model

341 were shown in Figure S18b and Figure 4c, respectively. $C_7H_7NO_3$ with about 72% of 6-methyl-2-

342 nitrophenol and 28% of 4-methyl-nitrophenol was directly generated from the reaction of TOL1O

343 + NO_2, MXYL1O + NO_2, and PXYL1O + NO_2 (Scheme S2), and was dominated by the first

344 pathway (75%). TOL1O, MXYL1O, and PXYL1O were photochemical products exhibiting their

345 highest concentration at noontime, while NO_2 was higher in the morning and evening (Figure 4b).

The diurnal patterns of TOL1O, MXYL1O, PXYL1O, and NO_2 resulted in the double peaks of the production rate of $C_7H_7NO_3$ in the daytime. Among the sources of TOL1O (Figure 4d), the reaction between *o*-methylphenyl peroxide (OXYL1O2) and NO seems to be the dominant pathway. However, TOL1O could quickly transform into OXYL1O2 via TOL1O+O_3 reaction in turn. The net production rate of TOL1O from OXYL1O2 ($P_{net\text{-}OXYL1O2}$) was lower than 1.9 pptv/h. The reaction of cresol+ NO_3• also contributed to the formation of TOL1O, and its highest production rate (4.2 pptv/h) and highest contribution (55%) was reached at around 16:00 and 17:00, respectively. It was noted that the high contribution of cresol + NO_3• to TOL1O presented in the daytime rather than at nighttime as expected. This was because cresol was a photochemical product, and though NO_3 was a main nocturnal oxidant, its concentration still could reach around 10^6 molecule/cm^3 in the daytime. The contribution of cresol + NO_3• was even higher than that of cresol + •OH to TOL1O, which can be explained by the following reasons. The reaction rate for cresol + NO_3• is 1.1~1.4×10^{-11} cm^3 $molecule^{-1}$ s^{-1}, which is only a little bit slower than the reaction rate of cresol + •OH (4.32~5.88×10^{-11} cm^3 $molecule^{-1}$ s^{-1}) [27, 66]. However, the yield of TOL1O in cresol + NO_3• (0.391) was much higher than that in cresol + •OH (0.073). It leads to a noticeable role of cresol + NO_3• on $C_7H_7NO_3$ formation in the daytime, especially in the afternoon.

The bi-modal pattern of observed $C_7H_7NO_3$ points to a fast consumption pathway offset the high production rate in the noontime. As shown in Figure 4c, photolysis was the dominant sink of $C_7H_7NO_3$ in the daytime associated with solar radiation and exceeded the production rates of $C_7H_7NO_3$ in the noontime. Hence, the net production rate of $C_7H_7NO_3$ increased after sunrise and

then decreased to negative value at noontime, followed by another increase in the afternoon. NO_3• started to increase at around 16:00 and made a significant contribution to $C_7H_7NO_3$ loss at around 17:00-20:00, which significantly contributed to the di-NPs formation in the evening, as discussed afterward. Moreover, the deposition of $C_7H_7NO_3$ also started to increase after sunset due to the decrease of the boundary layer. Because of the gradually weakened photochemical formation and the increased consumption caused by NO_3• and deposition in the evening, a sharp decrease of $C_7H_7NO_3$ started at 17:00-18:00. Consequently, the appearance of double peaks of $C_7H_7NO_3$ was attributed to the complex competition of the consumption of $C_7H_7NO_3$ by photolysis, NO_3• and deposition with the photochemical production from TOL1O+NO_2, MXYL1O+NO_2 and PXYL1O+NO_2. A similar budget analysis of $C_6H_5NO_3$ was provided in SI.

As gas-particle partitioning could also affect the variation of gaseous NPs, we also included this process in our simulation. Its contribution to NPs was not plotted in the budget figure but has been included in the calculation of net NPs production. The simulated average concentrations of particulate $C_6H_5NO_3$ and $C_7H_7NO_3$ from the gas-particle partitioning were 0.16 and 0.02 ng/m^3, respectively, within the concentration range of the particulate NPs observed at Hong Kong [18]. The particulate $C_6H_5NO_3$ and $C_7H_7NO_3$ only accounted for a small fraction of the total NPs, which highlights the importance of gaseous NPs detection to complete the understanding of NPs in the atmosphere.

Box model simulation with the additional constraint of observed mono-NPs was performed to analyze the budget of di-NPs. The simulated results for $C_6H_4N_2O_5$ and $C_7H_6N_2O_5$ were showed in

Figure S20a and S21a, which agreed reasonably with the observations. Nitrophenoxy (NPHEN1O) + NO_2 and methyl-nitrophenoxy (NCRES1O) + NO_2 were the direct pathways for the generation of $C_6H_4N_2O_5$ and $C_7H_6N_2O_5$, respectively. It was noted that significant production of $C_6H_4N_2O_5$ and $C_7H_6N_2O_5$ also occurred in the daytime rather than only in the nighttime, as directly observed in their concentration changes (Figure 4e, S21b). However, the daytime productions were offset by the fast photolysis loss during the daytime, resulting in a net loss rate in the daytime. The daytime production of those di-NPs was attributed to the noon peaks of NPHEN1O and NCRES1O (Figure S20b, S21c). Same as $C_7H_7NO_3$, the net contribution of nitro-phenylperoxy (NPHEN1O2) to NPHEN1O and nitro-methylphenyl peroxide (NCRES1O2) to NCRES1O were low owing to the conversion of NPHEN1O to NPHEN1O2 and NCRES1O to NCRES1O2 in turn with O_3 presented. The oxidation of related mono-NPs by •OH was an important source for NPHEN1O and NCRES1O formation in the daytime. With the decreased solar radiation and the increase of NO_3• concentration in the evening, the oxidation of mono-NPs by NO_3• became dominant, accounting for 68% and 66% of the formation of NPHEN1O and NCRES1O for the whole night (Figure 4f, 21d). Without the photolysis loss after sunset, this NO_3 oxidation pathway contributed to a positive net production rate of $C_6H_4N_2O_5$ and $C_7H_6N_2O_5$ (up to 0.43 and 0.46 pptv/hr, respectively), leading to the accumulation of their concentrations during the nighttime. The simulated average concentrations of $C_6H_4N_2O_5$ and $C_7H_6N_2O_5$ in particle phase from gas-particle partitioning were 0.37 and 0.53 ng/m^3, respectively, which were higher than the particulate $C_6H_5NO_3$ and $C_7H_7NO_3$ owing to the simulated lower saturated vapor pressures.

Aqueous-phase formation of NPs, not considered in the model, should play a minor role in the $C_6H_5NO_3$ and $C_7H_7NO_3$ formation due to the low average liquid water content of aerosol (1.5×10^{-11}) [67]. The low particulate $C_6H_5NO_3$ and $C_7H_7NO_3$ concentrations, obtained either from the simulated or the reported value also reduced the possibility of aqueous-phase formation for $C_6H_4N_2O_5$ and $C_7H_6N_2O_5$.

3.4 The photochemical impacts of high NPs in background air

HONO has been proved to be an important product from the photolysis of NPs [6, 7, 30]. The elevated daytime concentration and formation rate of NPs observed in this study may significantly impact the daytime HONO formation. Here, the production of HONO from the photolysis of NPs (PNPs) was calculated and was compared with other reported important sources of HONO, including the homogeneous reaction of OH+NO (OH+NO), the heterogeneous reaction of NO_2 on aerosol (Het-NO_2), the light-enhanced heterogeneous reaction of NO_2 on aerosol ($Het_{h\nu}$-NO_2), and the photolysis of particle nitrate (PNO_3^-). As shown in Figure 5a and S22, the average peak production rate of HONO from PNPs was 16.9 pptv/h, which was lower than that from NO+OH (116.1 pptv/h) and PNO_3^- (134.7 pptv/h) but was higher than the heterogeneous production (lower than 2.8 pptv/h). The highest production rate of NO+OH appeared at around 10:00 am, determined by the diurnal variation of NO and OH radicals. NO emitted from vehicles in the urban clusters would transport to the site and reach its peak value during 8:00-10:00 am, while the concentration of OH radical was mostly dependent on the solar radiation. The diurnal patterns of the HONO production from PNPs and PNO_3^- were similar, with a high peak value appearing at noon. The observed high

and broad NPs peaks in the afternoon provide a more persistent source for HONO formation, which results in the fraction of PNPs to HONO formation increased in the afternoon (Figure 5b). The contribution of NPs photolysis to HONO formation was higher than 10% after noon and reached 24 % at 16:00. The reported average concentration of HONO at the same site in the similar season of 2012 was 126±95 pptv [40]. The photolysis of NPs could be an important source for afternoon HONO formation and even OH radicals, which could help explain the unknown HONO source/mechanism and increasing atmospheric oxidation capacity in this and other coastal background regions. The sustained photochemical and nocturnal oxidations of precursors in the outflow of Asian continental air, especially the NO_3 oxidation in NOx-rich air, could produce abundant nitro-aromatic and organic nitrate species, which can significantly affect the atmospheric chemistry and regional air quality in the background and marine regions.

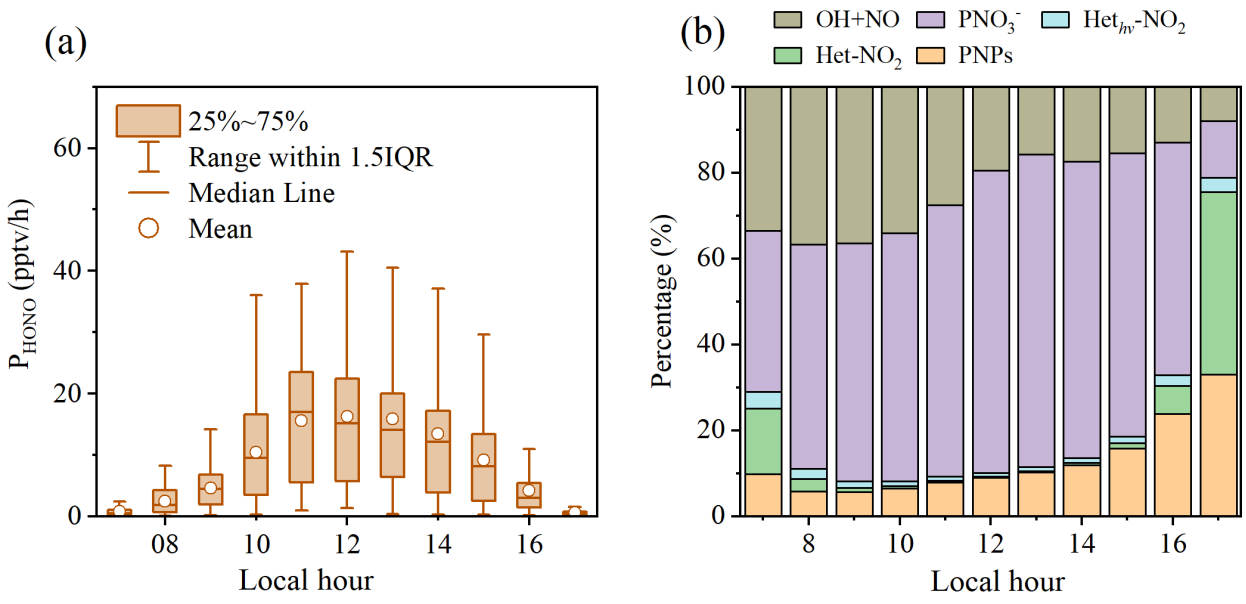

Figure 5. Production rate of HONO from the photolysis of nitrophenols (a), and the fraction of homogeneous reaction OH+NO, photolysis of particle nitrate (PNO_3^-), light-enhanced

heterogeneous reaction of NO_2 on aerosol ($Het_{h\nu}$-NO_2), heterogeneous reaction of NO_2 on aerosol (Het-NO_2), photolysis of nitrophenols (PNPs) to HONO formation (11.10-12.3) (b). IQR was inter quartile range. A unit yield of HONO was assumed in the NPs photolysis, and the photolysis rates of 1.4% of J_{NO2} for $C_6H_5NO_3$ and $C_6H_4N_2O_5$ and 5% of J_{NO2} for other NPs were adopted based on the simulation results and previous studies [29, 30, 63].

Associated Content

Supporting Information.

The following files are available on the ACS Publications website. HR-Tof-CIMS instrument settings; Box model setting; Budget analysis; Detail information of the site; High-resolution peak fitting; Calibration of $C_6H_5NO_3$; Overall results of other parameters; Time series of NPs; Correlations among NPs and related pollutants; Clusters of 72 h backward trajectories; Diurnal variations; Correlations between NPs and levoglucosan/CO; Secondary formation fractions of NPs; Time series and correlations of ΔO_3 and ΔNPs; Concentration of mono-NPs and di-NPs as a function of related precursors; Distribution of di-NPs and Cl-NPs as a function of NO_2; Transformation of di-NPs from mono-NPs; Reaction mechanisms of NPs; Simulations and budget analysis of NPs; HONO production ; Concentration of NPs and compounds input into the model (PDF).

Author Information

Corresponding Author

*Zhe Wang: z.wang@ust.hk

Notes

The authors declare no competing financial interest.

Acknowledgment

This study is supported by the Research Grants Council (RGC) of Hong Kong Special Administrative Region, China (T24-504/17-N), French ANR/RGC Joint Research Scheme (project A-PolyU502/16-SEAM), National Natural Science Foundation of China (91744204, 41875165, 42122062), and Hong Kong Environment and Conservation Fund (project 125/2020). The authors would like to acknowledge the HKPolyU University Research Facility in Chemical and Environmental Analysis (UCEA) for the equipment support, and Hong Kong Environmental Protection Department for providing access to the Cape D'Aguilar Supersite AQMS and for sharing the trace gases, particles and VOCs data at the Supersite.

References

1. Harrison, M. A. J.; Barra, S.; Borghesi, D.; Vione, D.; Arsene, C.; Iulian Olariu, R. Nitrated phenols in the atmosphere: a review. *Atmos. Environ.* **2005,** *39* (2), 231-248.

2. Xie, M.; Chen, X.; Hays, M. D.; Lewandowski, M.; Offenberg, J.; Kleindienst, T. E.; Holder, A. L. Light absorption of secondary organic aerosol: Composition and contribution of nitroaromatic compounds. *Environ. Sci. Technol.* **2017,** *51* (20), 11607-11616.

3. Teich, M.; van Pinxteren, D.; Wang, M.; Kecorius, S.; Wang, Z.; Müller, T.; Močnik, G.; Herrmann, H. Contributions of nitrated aromatic compounds to the light absorption of water-soluble and particulate brown carbon in different atmospheric environments in Germany and China. *Atmos. Chem. Phys.* **2017,** *17* (3), 1653-1672.

4. Li, C.; He, Q.; Hettiyadura, A. P. S.; Kafer, U.; Shmul, G.; Meidan, D.; Zimmermann, R.; Brown, S. S.; George, C.; Laskin, A.; Rudich, Y. Formation of secondary brown carbon in biomass burning aerosol proxies through NO_3 radical reactions. *Environ. Sci. Technol.* **2020,** *54* (3), 1395-1405.

5. Mohr, C.; Lopez-Hilfiker, F. D.; Zotter, P.; Prevot, A. S.; Xu, L.; Ng, N. L.; Herndon, S. C.; Williams, L. R.; Franklin, J. P.; Zahniser, M. S.; Worsnop, D. R.; Knighton, W. B.; Aiken, A. C.; Gorkowski, K. J.; Dubey, M. K.; Allan, J. D.; Thornton, J. A. Contribution of nitrated phenols to wood burning brown carbon light absorption in Detling, United Kingdom during winter time. *Environ. Sci. Technol.* **2013,** *47* (12), 6316-6324.

6. Sangwan, M.; Zhu, L. Role of methyl-2-nitrophenol photolysis as a potential source of OH radicals in the polluted atmosphere: Implications from laboratory investigation. *J. Phys. Chem. A* **2018,** *122* (7), 1861-1872.

7. Sangwan, M.; Zhu, L. Absorption cross sections of 2-nitrophenol in the 295-400 nm region and photolysis of 2-nitrophenol at 308 and 351 nm. *J. Phys. Chem. A* **2016,** *120* (50), 9958-9967.

8. Cerullo, G.; Nitta, Y.; Schalk, O.; Kaneshima, K.; Sekikawa, T.; Ogilvie, J.; Kärtner, F.; Khalil, M.; Li, R. Ultrafast photolysis of *o*-nitrophenol studied by time-resolved photoelectron spectroscopy. *EPJ Web of Conferences* **2019,** *205*, 09022.

9. Bejan, I.; Abd-el-Aal, Y.; Barnes, I.; Benter, T.; Bohn, B.; Wiesen, P.; Kleffmann, J. The photolysis of *ortho*-nitrophenols: a new gas phase source of HONO. *Phys. Chem. Chem. Phys.* **2006,** *8* (17), 2028-2035.

10. Wang, Y.; Hu, M.; Wang, Y.; Zheng, J.; Shang, D.; Yang, Y.; Liu, Y.; Li, X.; Tang, R.; Zhu, W.; Du, Z.; Wu, Y.; Guo, S.; Wu, Z.; Lou, S.; Hallquist, M.; Yu, J. Z. The formation of nitro-aromatic compounds under high NOx and anthropogenic VOC conditions in urban Beijing, China. *Atmos. Chem. Phys.* **2019,** *19* (11), 7649-7665.

11. Li, M.; Wang, X.; Lu, C.; Li, R.; Zhang, J.; Dong, S.; Yang, L.; Xue, L.; Chen, J.; Wang, W. Nitrated phenols and the phenolic precursors in the atmosphere in urban Jinan, China. *Sci. Total Environ.* **2020,** *714*, 136760.

12. Delhomme, O.; Morville, S.; Millet, M. Seasonal and diurnal variations of atmospheric concentrations of phenols and nitrophenols measured in the Strasbourg area, France. *Atmos. Pollut. Res.* **2010,** *1* (1), 16-22.

13. Lu, C.; Wang, X.; Li, R.; Gu, R.; Zhang, Y.; Li, W.; Gao, R.; Chen, B.; Xue, L.; Wang, W. Emissions of fine particulate nitrated phenols from residential coal combustion in China. *Atmos. Environ.* **2019,** *203*, 10-17.

14. Wang, X.; Gu, R.; Wang, L.; Xu, W.; Zhang, Y.; Chen, B.; Li, W.; Xue, L.; Chen, J.; Wang, W. Emissions of fine particulate nitrated phenols from the burning of five common types of biomass. *Environ. Pollut.* **2017,** *230*, 405-412.

15. Lu, C.; Wang, X.; Dong, S.; Zhang, J.; Li, J.; Zhao, Y.; Liang, Y.; Xue, L.; Xie, H.; Zhang, Q.; Wang, W. Emissions of fine particulate nitrated phenols from various on-road vehicles in China. *Environ. Res.* **2019,** *179*, 108709.

16. Ikemori, F.; Nakayama, T.; Hasegawa, H. Characterization and possible sources of nitrated mono- and di-aromatic hydrocarbons containing hydroxyl and/or carboxyl functional groups in ambient particles in Nagoya, Japan. *Atmos. Environ.* **2019,** *211*, 91-102.

17. Yoshiteru Iinuma; Olaf Böge; Ricarda Gräfe; Herrmann, H. Methyl-nitrocatechols: atmospheric tracer compounds for biomass burning secondary organic aerosols. *Environ. Sci. Technol.* **2010,** *44*, 8453-8459.

18. Chow, K. S.; Huang, X. H. H.; Yu, J. Z. Quantification of nitroaromatic compounds in atmospheric fine particulate matter in Hong Kong over 3 years: field measurement evidence for secondary formation derived from biomass burning emissions. *Environ. Chem.* **2016,** *13* (4), 665.

19. Bolzacchini, E.; Bruschi, M.; Hjorth, J.; Meinardi, S.; Orlandi, M.; Rindone, B.; Rosenbohm, E. Gas-phase reaction of phenol with NO_3. *Environ. Sci.Technol.* **2001,** *35*, 1791-1797.

20. Olariu, R. I.; Barnes, I.; Bejan, I.; Arsene, C.; Vione, D.; Klotz, B.; Becker, K. H. FT-IR product study of the reactions of NO_3 radicals with *ortho*-, *meta*-, and *para*-cresol. *Environ. Sci. Technol.* **2013,** *47* (14), 7729-7738.

21. Zhang, H.; Yang, B.; Wang, Y.; Shu, J.; Zhang, P.; Ma, P.; Li, Z. Gas-phase reactions of methoxyphenols with NO_3 radicals: Kinetics, products, and mechanisms. *J. Phys. Chem. A* **2016,** *120* (8), 1213-1221.

22. Xu, C.; Wang, L. Atmospheric oxidation mechanism of phenol initiated by OH radical. *J. Phys. Chem. A* **2013,** *117* (11), 2358-2364.

23. Atkinson, R.; Aschmann, S. M.; Winer, A. M. Kinetics of the reactions of NO_3 radicals with a series of aromatic compounds. *Environ. Sci. Technol.* **1987,** *21* (11), 1123-1126.

24. Atkinson, R.; Aschmann, S. M.; Arey, J. Reactions of OH and NO_3 radicals with phenol, cresols, and 2-nitrophenol at 296 ± 2 K. *Environ. Sci. Technol.* **1992,** *26*, 1397-1403.

25. Finewax, Z.; de Gouw, J. A.; Ziemann, P. J. Identification and quantification of 4-nitrocatechol formed from OH and NO_3 radical-initiated reactions of catechol in air in the presence of NO_x: Implications for secondary organic aerosol formation from biomass burning. *Environ. Sci. Technol.* **2018,** *52* (4), 1981-1989.

26. Ji, Y.; Zhao, J.; Terazono, H.; Misawa, K.; Levitt, N. P.; Li, Y.; Lin, Y.; Peng, J.; Wang, Y.; Duan, L.; Pan, B.; Zhang, F.; Feng, X.; An, T.; Marrero-Ortiz, W.; Secrest, J.; Zhang, A. L.; Shibuya, K.; Molina, M. J.; Zhang, R. Reassessing the atmospheric oxidation mechanism of toluene. *Proc. Natl. Acad. Sci. USA* **2017,** *114* (31), 8169-8174.

27. Lars P. Thuner; Perla Bardini; Gerard J. Rea; Wenger, J. C. Kinetics of the gas-phase reactions of OH and NO_3 radicals with dimethylphenols. *J. Phys. Chem. A* **2004,** *108*, 11019-11025.

28. Vione, D.; Maurino, V.; Minero, C.; Pelizzetti, E. Aqueous atmospheric chemistry: Formation of 2,4-dinitrophenol upon nitration of 2-nitrophenol and 4-nitrophenol in solution. *Environ. Sci. Technol.* **2005,** *39*, 7921-7931.

29. Yuan, B.; Liggio, J.; Wentzell, J.; Li, S.-M.; Stark, H.; Roberts, J. M.; Gilman, J.; Lerner, B.; Warneke, C.; Li, R.; Leithead, A.; Osthoff, H. D.; Wild, R.; Brown, S. S.; de Gouw, J. A. Secondary formation of nitrated phenols: insights from observations during the Uintah Basin Winter Ozone Study (UBWOS) 2014. *Atmos. Chem. Phys.* **2016,** *16* (4), 2139-2153.

30. Bejan, I.; Barnes, I.; Olariu, R.; Zhou, S.; Wiesen, P.; Benter, T. Investigations on the gas-phase photolysis and OH radical kinetics of methyl-2-nitrophenols. *Phys. Chem. Chem. Phys.* **2007,** *9* (42), 5686-5692.

31. Bejan, I.; Duncianu, M.; Olariu, R.; Barnes, I.; Seakins, P. W.; Wiesen, P. Kinetic study of the gas-phase reactions of chlorine atoms with 2-chlorophenol, 2-nitrophenol, and four methyl-2-nitrophenol isomers. *J. Phys. Chem. A* **2015,** *119* (20), 4735-4745.

32. Rubio, M. A.; Lissi, E.; Herrera, N.; Perez, V.; Fuentes, N. Phenol and nitrophenols in the air and dew waters of Santiago de Chile. *Chemosphere* **2012,** *86* (10), 1035-1039.

33. Cecinato, A.; Di Palo, V.; Pomata, D.; Tomasi Sciano, M. C.; Possanzini, M. Measurement of phase-distributed nitrophenols in Rome ambient air. *Chemosphere* **2005,** *59* (5), 679-683.

34. Cheng, X.; Chen, Q.; Li, Y.; Huang, G.; Liu, Y.; Lu, S.; Zheng, Y.; Qiu, W.; Lu, K.; Qiu, X.; Bianchi, F.; Yan, C.; Yuan, B.; Shao, M.; Wang, Z.; Canagaratna, M. R.; Zhu, T.; Wu, Y.; Zeng, L. Secondary production of gaseous nitrated phenols in polluted urban environments. *Environ. Sci. Technol.* **2021,** *55* (8), 4410-4419.

35. Song, K.; Guo, S.; Wang, H.; Yu, Y.; Wang, H.; Tang, R.; Xia, S.; Gong, Y.; Wan, Z.; Lv, D.; Tan, R.; Zhu, W.; Shen, R.; Li, X.; Yu, X.; Chen, S.; Zeng, L.; Huang, X. Measurement report: Online measurement of gas-phase nitrated phenols utilizing a CI-LToF-MS: primary sources and secondary formation. *Atmos. Chem. Phys.* **2021,** *21* (10), 7917-7932.

581 36. Salvador, C. M. G.; Tang, R.; Priestley, M.; Li, L.; Tsiligiannis, E.; Le Breton, M.; Zhu, W.;
582 Zeng, L.; Wang, H.; Yu, Y.; Hu, M.; Guo, S.; Hallquist, M. Ambient nitro-aromatic compounds –
583 biomass burning versus secondary formation in rural China. *Atmos. Chem. Phys.* 2021, *21* (3),
584 1389-1406.

585 37. Wang, H.; Gao, Y.; Wang, S.; Wu, X.; Liu, Y.; Li, X.; Huang, D.; Lou, S.; Wu, Z.; Guo, S.;
586 Jing, S.; Li, Y.; Huang, C.; Tyndall, G. S.; Orlando, J. J.; Zhang, X. Atmospheric processing of
587 nitrophenols and nitrocresols from biomass burning emissions. *J. Geophys. Res.: Atmos.* 2020,
588 *125* (22), e2020JD033401.

589 38. Lyu, X.; Guo, H.; Yao, D.; Lu, H.; Huo, Y.; Xu, W.; Kreisberg, N.; Goldstein, A. H.; Jayne,
590 J.; Worsnop, D.; Tan, Y.; Lee, S. C.; Wang, T. In situ measurements of molecular markers facilitate
591 understanding of dynamic sources of atmospheric organic aerosols. *Environ. Sci. Technol.* 2020,
592 *54* (18), 11058-11069.

593 39. Ding, A.; Wang, T.; Fu, C. Transport characteristics and origins of carbon monoxide and
594 ozone in Hong Kong, South China. *J. Geophys. Res.: Atmos.* 2013, *118* (16), 9475-9488.

595 40. Zha, Q.; Xue, L.; Wang, T.; Xu, Z.; Yeung, C.; Louie, P. K. K.; Luk, C. W. Y. Large
596 conversion rates of NO_2 to HNO_2 observed in air masses from the South China Sea: Evidence of
597 strong production at sea surface? *Geophys. Res. Lett.* 2014, *41* (21), 7710-7715.

598 41. Yu, C.; Wang, Z.; Xia, M.; Fu, X.; Wang, W.; Tham, Y. J.; Chen, T.; Zheng, P.; Li, H.; Shan,
599 Y.; Wang, X.; Xue, L.; Zhou, Y.; Yue, D.; Ou, Y.; Gao, J.; Lu, K.; Brown, S. S.; Zhang, Y.; Wang,

T. Heterogeneous N_2O_5 reactions on atmospheric aerosols at four Chinese sites: improving model representation of uptake parameters. *Atmos. Chem. Phys.* **2020,** *20* (7), 4367-4378.

42. He, Z.; Wang, X.; Ling, Z.; Zhao, J.; Guo, H.; Shao, M.; Wang, Z. Contributions of different anthropogenic volatile organic compound sources to ozone formation at a receptor site in the Pearl River Delta region and its policy implications. *Atmos. Chem. Phys.* **2019,** *19* (13), 8801-8816.

43. Ling, Z.; Xie, Q.; Shao, M.; Wang, Z.; Wang, T.; Guo, H.; Wang, X. Formation and sink of glyoxal and methylglyoxal in a polluted subtropical environment: observation-based photochemical analysis and impact evaluation. *Atmos. Chem. Phys.* **2020,** *20* (19), 11451-11467.

44. Johnson, D.; Jenkin, M. E.; Wirtz, K.; Martin-Reviejo, M. Simulating the formation of secondary organic aerosol from the photooxidation of aromatic hydrocarbons. *Environ. Chem.* **2005,** *2* (1), 35.

45. Belloli, R.; Bolzacchini, E.; Clerici, L.; Rindone, B.; Sesana, G.; Librando, V. Nitrophenols in air and rainwater. *Environ. Eng. Sci.* **2006,** *23* (2), 405-415.

46. Zhang, Q.; Sarkar, S.; Wang, X.; Zhang, J.; Mao, J.; Yang, L.; Shi, Y.; Jia, S. Evaluation of factors influencing secondary organic carbon (SOC) estimation by CO and EC tracer methods. *Sci. Total Environ.* **2019,** *686*, 915-930.

47. Li, K.; Li, J.; Tong, S.; Wang, W.; Huang, R.-J.; Ge, M. Characteristics of wintertime VOCs in suburban and urban Beijing: concentrations, emission ratios, and festival effects. *Atmos. Chem. Phys.* **2019,** *19* (12), 8021-8036.

48. Jenkin, M. E.; Saunders, S. M.; Wagner, V.; Pilling, M. J. Protocol for the development of the Master ChemicalMechanism, MCMv3 (Part B): Tropospheric degradation of aromatic volatile organic compounds. *Atmos. Chem. Phys.* **2003,** *3*, 181–193.

49. Cantrell, C. A.; Davidson, J. A.; McDaniel, A. H.; Shetter, R. E.; Calvert, J. G. The equilibrium constant for $N_2O_5 \rightleftarrows NO_2+NO_3$: Absolute determination by direct measurement from 243 to 397 K. *J. Chem. Phys.* **1988,** *88* (8), 4997-5006.

50. Osthoff, H. D.; Pilling, M. J.; Ravishankara, A. R.; Brown, S. S. Temperature dependence of the NO_3 absorption cross-section above 298 K and determination of the equilibrium constant for $NO_3 + NO_2 <--> N_2O_5$ at atmospherically relevant conditions. *Phys. Chem. Chem. Phys.* **2007,** *9* (43), 5785-5793.

51. Wang, H.; Lou, S.; Huang, C.; Qiao, L.; Tang, X.; Chen, C.; Zeng, L.; Wang, Q.; Zhou, M.; Lu, S.; Yu, X. Source profiles of volatile organic compounds from biomass burning in Yangtze River Delta, China. *Aerosol Air Qual. Res.* **2014,** *14* (3), 818-828.

52. Li, L.; Chen, Y.; Zeng, L.; Shao, M.; Xie, S.; Chen, W.; Lu, S.; Wu, Y.; Cao, W. Biomass burning contribution to ambient volatile organic compounds (VOCs) in the Chengdu–Chongqing Region (CCR), China. *Atmos. Environ.* **2014,** *99*, 403-410.

53. Zhu, Y.; Yang, L.; Chen, J.; Wang, X.; Xue, L.; Sui, X.; Wen, L.; Xu, C.; Yao, L.; Zhang, J.; Shao, M.; Lu, S.; Wang, W. Characteristics of ambient volatile organic compounds and the influence of biomass burning at a rural site in Northern China during summer 2013. *Atmos. Environ.* **2016,** *124*, 156-165.

54. Wu, R.; Wang, S.; Wang, L. Atmospheric oxidation mechanism of chlorobenzene. *Chemosphere* **2014,** *111*, 537-544.

55. Bryukov, M. G.; Knyazev, V. D.; William M. Gehling, J.; Dellinger, B. Kinetics of the gas-phase reaction of OH with chlorobenzene. *J. Phys. Chem. A* **2009,** *113*, 10452–10459.

56. Atkinson, R.; Aschmann, S. M.; Winer, A. M.; James N. Pitts, J. Atmospheric gas phase loss processes for chlorobenzene, benzotrifluoride, and 4-chlorobenzotrifluoride, and generalization of predictive techniques for atmospheric lifetimes of aromatic compounds. *Arch. Environ. Contam. Toxicol.* **1985,** *14*, 417-425.

57. Chiron, S.; Minero, C.; Vione, D. Occurrence of 2,4-dichlorophenol and of 2,4-dichloro-6-nitrophenol in the Rhône River Delta (Southern France). *Environ. Sci. Technol.* **2007,** *41* (9), 3127–3133.

58. Olaniran, A. O.; Igbinosa, E. O. Chlorophenols and other related derivatives of environmental concern: properties, distribution and microbial degradation processes. *Chemosphere* **2011,** *83* (10), 1297-1306.

59. Bunce, N. J.; Nakai, J. S. Atmospheric chemistry of chlorinated phenols. *JAPCA* **1989,** *39*(6), 820-823.

60. K. Tonokura; Y. Norikane; M. Koshi; Y. Nakano; S. Nakamichi; M. Goto; S. Hashimoto; M. Kawasaki; M. P. Sulbaek Andersen; M. D. Hurley; Wallington, T. J. Cavity ring-down study of the visible absorption spectrum of the phenyl radical and kinetics of its reactions with Cl, Br, Cl_2, and O_2. *J. Phys. Chem. A* **2002,** *106* (24), 5908-5917.

61. O. Sokolov; M. D. Hurley; T. J. Wallington; E. W. Kaiser; J. Platz; O. J. Nielsen; F. Berho; M.-T. Rayez; Lesclaux, R. Kinetics and mechanism of the gas-phase reaction of Cl atoms with benzene. *J. Phys. Chem. A* **1998,** *102*, 10671-10681.

62. Xue, L. K.; Saunders, S. M.; Wang, T.; Gao, R.; Wang, X. F.; Zhang, Q. Z.; Wang, W. X. Development of a chlorine chemistry module for the Master Chemical Mechanism. *Geosci. Model. Dev.* **2015,** *8* (10), 3151-3162.

63. Bardini, P. Atmospheric chemistry of dimethylphenols & nitrophenols. Ph.D. thesis, University College Cork, 2006.

64. Palm, B. B.; Peng, Q.; Fredrickson, C. D.; Lee, B. H.; Garofalo, L. A.; Pothier, M. A.; Kreidenweis, S. M.; Farmer, D. K.; Pokhrel, R. P.; Shen, Y.; Murphy, S. M.; Permar, W.; Hu, L.; Campos, T. L.; Hall, S. R.; Ullmann, K.; Zhang, X.; Flocke, F.; Fischer, E. V.; Thornton, J. A. Quantification of organic aerosol and brown carbon evolution in fresh wildfire plumes. *Proc. Natl. Acad. Sci. USA* **2020,** *117* (47), 29469-29477.

672 65. Shiraiwa, M.; Selzle, K.; Yang, H.; Sosedova, Y.; Ammann, M.; Poschl, U. Multiphase
673 chemical kinetics of the nitration of aerosolized protein by ozone and nitrogen dioxide. *Environ.*
674 *Sci. Technol.* **2012,** *46* (12), 6672-6680.

675 66. Coeur-Tourneur, C.; Henry, F.; Janquin, M.-A.; Brutier, L. Gas-phase reaction of hydroxyl
676 radicals with *m*-,*o*- and *p*-cresol. *Int. J. Chem. Kinet.* **2006,** *38* (9), 553-562.

677 67. Harrison, M. A. J.; Heal, M. R.; Cape, J. N. Evaluation of the pathways of tropospheric
678 nitrophenol formation from benzene and phenol using a multiphase model. *Atmos. Chem. Phys.*
679 **2005,** *5*, 1679–1695.